GANIT: Journal of Bangladesh Mathematical Society

GANIT

GANIT*J. Bangladesh Math. Soc.*46.1(2026) 019–034
DOI: https://doi.org/10.3329/ganit.v46i1.91334

A Study on Virus-Host Cell Genetic Material Transport

Mst. Samira Khatun [a*]

[a] Department of Mathematics, Kishoreganj University, Kishoreganj 2300, Bangladesh

ABSTRACT

Viral dynamics are commonly modeled using systems of nonlinear ordinary differential equations to describe the interaction between target cells, infected cells, and free virus particles. The target cell–limited model has been extensively studied in the literature, where numerical solutions are typically obtained using fixed-step finite difference schemes such as the classical fourth-order Runge–Kutta (RK4) method. In this study, we solve the target cell–limited viral dynamics model using an embedded numerical scheme, namely the RKAHeM (4,4) method, which provides enhanced accuracy and error control. Numerical simulations are performed, and the obtained results show excellent agreement with previously reported solutions, thereby validating the effectiveness and robustness of the proposed method.

© 2026 Published by Bangladesh Mathematical Society
Received: February 15, 2026 **Accepted:** March 14, 2026 **Published Online:** June 30, 2026

Keywords: Target cell-limited model; virus-host cell interaction; RK (4, 4) method; RKAHeM (4, 4) technique.

*Corresponding Author. *Email Address:* samirak814@gmail.com

1. Introduction

Virus-host cell interactions are a Complex biological mechanism including binding to cells, entry, dissemination, and finally lytic or chronic infection [1]. As host-dependent pathogens, viruses are closely associated with host cells. Virus-host cell interactions not only allow the virus to use the cell for its own purposes but also provide the host cell with the means to fight viral infection. Due to the close relationship between host and viral processes, the sciences of cell biology and virology have often influenced each other [2]. It is well established that after entering a cell, a virus commandeers the host's cellular machinery to synthesize the viral proteins required for the replication of its genome. The perpetuation of a virus throughout an epidemic hinges on its ability to successfully bind to a host cell and deliver its genetic material—a payload that may consist of DNA, RNA, or protein. Once internalized, this material replicates, a phase during which the genome is also subject to potential mutations [3]. Numerous studies demonstrate how viruses have evolved to interfere with essential host proteins and signaling pathways, circumvent innate immune responses, and hijack basic cell signaling pathways. Considering these numerous studies together, it will be possible to advance our elucidation of virus-host interactions and give new avenues for the creation of targeted antiviral agents [4]. The economic burden of viral epidemics is twofold, combining the costs of diagnosis and treatment with lost productivity from absenteeism. It is of interest that the experimental quantification coupled with computational modeling may increase our

understanding of the within-host infection dynamics and may lead to important insights into viral pathogenesis, transmission, and disease progression. By simulating in vivo dynamics, these models offer a platform to identify potential drug targets, predict the necessary duration for a cure, and minimize associated treatment expenses. This study explains the viral dynamic model that includes the uninfected target cell, the infected virus-producing cell, and the quantities of free viruses. Numerous existing studies discussed the model and solved it by the steady-state approximation method and numerically by the Runge- Kutta (4, 4) approximation. However, in the case of our work, we solve it by the embedded system, namely the RKAHeM (4, 4) technique to accrue more accurate results with economic cost and computational cost.

2. The basic target cell-limited model

A classic mathematical formulation for viral dynamics that illustrates the interaction of a virus with target cells can be given through the following equations [5]:

$$\frac{dT}{dt} = \lambda - \rho T - \beta TV \tag{1}$$

$$\frac{dI}{dt} = \beta TV - \delta I \tag{2}$$

$$\frac{dV}{dt} = bI - \gamma V \tag{3}$$

In Eqs. (1)-(3), T indicates the uninfected target-cell population, I refers to the cohort of cells actively harboring the virus, and V the free virus, and t denotes time. It is assumed that λ is the constant rate at which uninfected target cells (T) are produced and die at rate ρ. When the virus V attack the uninfected target cell T at a constant infectivity rate β, then it becomes an infected virus-producing cell and produces viruses at rate b**.** Due to the effect of immunological clearance, or apoptotic cell death, infected cells (Idie with a rate constant of δ and the viruses are removed at a rate γ from the cell.

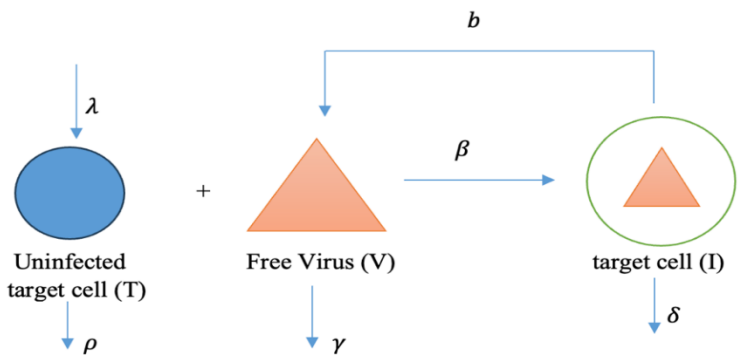

Figure 1: Visual representation of the target cell-limited model.

For the above model, we assume that the viral infection is noncytopathic, i.e., the death rate of the infected and uninfected cells is equal, and, therefore, we take $\rho = \delta$ in the analysis.

The system of equations as they stand cannot be solved analytically. The resort has been taken to a numerical technique. But this treatment requires the equations to be normalized. To non-dimensionalize the equations, we propose the following dimensionless parameters.

$x(\tau;\epsilon) = \frac{\rho}{\lambda}T(t)$, $y(\tau;\epsilon) = \frac{\rho}{\lambda}I(t)$, $v(\tau;\epsilon) = \frac{\beta}{\rho}V(t)$, $\tau = \rho t$, $\epsilon = \frac{\rho}{\gamma}$, $R_0 = \frac{\lambda\beta b}{\rho\delta\gamma}$.

The above non-dimensional equations bring Eqs. $(1) - (3)$ to the following form:

$$\frac{dx}{d\tau} = 1 - x - xv \tag{4}$$

$$\frac{dy}{d\tau} = xv - y \tag{5}$$

$$\frac{dv}{d\tau} = R_0 y - v \tag{6}$$

2.1. Theoretical Justifications for Positivity and Boundedness

The target cell-limited viral dynamics model defined by Equations. $(1) - (3)$ satisfies fundamental mathematical properties that ensure its biological validity.

Positivity**:** All state variables $T(t)$, $I(t)$, and $V(t)$ remain non-negative for all $t \geq 0$ given non-negative initial conditions.

Boundedness: All solutions are uniformly bounded in $\mathbb{R}^3_+$ with explicit upper bounds derived from system parameters.

These properties confirm that the model produces biologically plausible results (no negative cell populations or viral loads) and that solutions do not blow up in finite time.

Definition**:** The system is said to be positive if for any initial condition $(T_0, I_0, V_0) \in \mathbb{R}^3_+$ the corresponding solution $(T(t), I(t), V(t))$ remains in $\mathbb{R}^3_+$ for all $t \geq 0$.

Definition: The system is said to be bounded if there exists a compact set $K \subset \mathbb{R}^3_+$ such that all solutions eventually enter and remain in K.

2.1.1. Positivity Analysis

Theorem 1: For any initial condition $(T_0, I_0, V_0) \in \mathbb{R}^3_+$ the solution $(T(t), I(t), V(t))$ of system (1) remains non-negative for all $t \geq 0$.

Proof**:**

We prove positivity component by component using the method of separation of variables and the structure of the differential equations.

Step 1: Positivity of $T(t)$: Consider the differential equation for T is

$$\frac{dT}{dt} = \lambda - \rho T - \beta T V \geq -(\rho + \beta V)T$$

since $\lambda \geq 0$. This is a differential inequality. Define $U(t) = T(t)$. Then

$$\frac{dU}{dt} \geq -(\rho + \beta V(t))U$$

Solving this inequality

$$U(t) \geq U(0) exp\left(-\int_0^t (\rho + \beta V(s))ds\right) U(0) \geq 0$$

since $U(0) = T_0 \geq 0$ and the exponential term is always positive. Therefore, $T(t) \geq 0$ for all $t \geq 0$.

Step 2: Positivity of $I(t)$: The equation for I can be written as

$$\frac{dI}{dt} = \beta T V - \delta I$$

This is a linear first-order equation with a non-negative forcing term (since $T \geq 0$ and $V \geq 0$ from Steps 1 and 3, though Step 3 depends on Step 2, we must be careful with circular reasoning). To avoid circularity, we solve explicitly:

$$I(t) = I_0 e^{-\delta t} + \int_0^t \beta T(s) V(s) e^{-\delta(t-s)}\, ds$$

Both terms are non-negative: the first term is non-negative because $I_0 \geq 0$ and the integrand is non-negative because $\beta > 0$, $T(s) \geq 0$ (from Step 1), and $V(s) \geq 0$ (which we will prove in Step 3). However, this creates a dependency: we need $V(s) \geq 0$ to prove $I(t) \geq 0$, and we need $I(s) \geq 0$ to prove $V(t) \geq 0$.

To resolve this circularity, we use a simultaneous positivity argument.

Lemma 1.1: For sufficiently small $t > 0$, both $I(t)$and $V(t)$ remain non-negative. By continuity of solutions, there exists $\epsilon > 0$ such that for $t \in [0, \epsilon]$, $V(t)$ remains close to $V_0 \geq 0$. If $V_0 > 0$, then $V(t) > 0$ for small t. If $V_0 = 0$, then $\frac{dV}{dt}(0) = bI_0 \geq 0$, so $V(t)$ cannot become negative

immediately. A similar argument holds for $I(t)$. Therefore, there exists an interval $[0, \epsilon)$ where both $I(t)$ and $V(t)$ are non-negative.

Step 3: Positivity of $V(t)$

Similarly, the equation for V gives:

$$\frac{dV}{dt} = \mathrm{bI} - \gamma \mathrm{V} \geq -\gamma V$$

since $bI \geq 0$ for $t \in [0, \epsilon)$ from Lemma 1.1. Solving we get

$$V(t) \geq V_0 e^{-\gamma t} \geq 0$$

for $t \in [0, \epsilon)$.

Step 4: Extension to All Time

We now have positivity on $[0, \epsilon)$. Let ϵ^* be the supremum of all ϵ for which positivity holds. Suppose $\epsilon^* < \infty$. Then at $t = \epsilon^*$, at least one component becomes zero. But the explicit formulas show that if a component becomes zero, its derivative is non-negative.

- If $T(\epsilon^*) = 0$, then $\frac{dT}{dt}(\epsilon^*) = \lambda > 0$ so T increases immediately, contradicting it being zero at an interior point.
- If $I(\epsilon^*) = 0$, then $\frac{dI}{dt}(\epsilon^*) = \beta \mathrm{T}(\epsilon^*)\mathrm{V}(\epsilon^*) \geq 0$.
- If $V(\epsilon^*) = 0$, then $\frac{dV}{dt}(\epsilon^*) = \mathrm{bI}(\epsilon^*) \geq 0$.

Therefore, the solution cannot leave the positive orthant. By continuation, positivity holds for all $t \geq 0$.

2.1.2. Boundedness Analysis

Theorem 2: All solutions of system (1) with non-negative initial conditions are uniformly bounded in $\mathbb{R}^3_+$. Specifically, there exists a positive constant M such that for any initial condition, $\lim_{t\to\infty} sup\left(T(t) + I(t) + V(t)\right) \leq M$.

Proof: We construct a Lyapunov-like function to establish boundedness.

Step 1: Boundedness of $T + I$

Consider the dynamics of total cell population $N = T + I$. Then

$$\frac{dN}{dt} = \frac{dT}{dt} + \frac{dI}{dt} = (\lambda - \rho \mathrm{T} - \beta \mathrm{TV}) + (\beta \mathrm{TV} - \delta \mathrm{I}) = \lambda - \rho \mathrm{T} - \delta \mathrm{I}$$

Since ρ and δ are positive, we have

$$\frac{dN}{dt} \leq \lambda - \min(\rho, \delta)(T + I) = \lambda - \mu N$$

where $\mu = min(\rho, \delta) > 0$.

Solving this differential inequality

$$N(t) \leq N(0)e^{-\mu \mathrm{t}} + \frac{\lambda}{\mu}(1 - e^{-\mu \mathrm{t}})$$

Therefore

$$\lim_{t\to\infty} supN(t) \leq \frac{\lambda}{\mu} = \frac{\lambda}{\min(\rho, \delta)}$$

Step 2: Boundedness of V

Now consider the viral dynamics. From the boundedness of I (since $I \leq N$), we have $I(t) \leq \frac{\lambda}{\mu} + \epsilon$ for large t. Then

$$\frac{dV}{dt} = \mathrm{bI} - \gamma \mathrm{V} \leq \mathrm{b}\left(\frac{\lambda}{\mu} + \epsilon\right) - \gamma \mathrm{V}$$

Solving this inequality, we get

$$V(t) \leq V(0)e^{-\gamma \mathrm{t}} + \frac{b}{\gamma}\left(\frac{\lambda}{\mu} + \epsilon\right)(1 - e^{-\gamma \mathrm{t}})$$

Thus

$$\lim_{t\to\infty} supV(t) \leq \frac{b\lambda}{\gamma\mu}.$$

Step 3: Construction of a Composite Bound:

Define the function $W(t) = T(t) + I(t) + \frac{\delta}{2b}V(t)$. Then

$$\frac{dW}{dt} = \frac{dT}{dt} + \frac{dI}{dt} + \frac{\delta}{2b}\frac{dV}{dt}$$

$$= (\lambda - \rho T - \beta TV) + (\beta TV - \delta I) + \frac{\delta}{2b}(bI - \gamma V)$$

$$= \lambda - \rho T - \delta I + \frac{\delta}{2}I - \frac{\delta\gamma}{2b}V$$

$$= \lambda - \rho T - \frac{\delta}{2}I - \frac{\delta\gamma}{2b}V$$

$$\leq \lambda - min\left(\rho, \frac{\delta}{2}, \frac{\delta\gamma}{2b}\right)W$$

Let $\eta = min\left(\rho, \frac{\delta}{2}, \frac{\delta\gamma}{2b}\right) > 0$. Then

$$\frac{dW}{dt} \leq \lambda - \eta W$$

Solving this we get

$$W(t) \leq W(0)e^{-\eta t} + \frac{\lambda}{\eta}(1 - e^{-\eta t})$$

Therefore

$$\lim_{t\to\infty} supW(t) \leq \frac{\lambda}{\eta}$$

Since $T + I + V \leq max(1, \frac{2b}{\delta})W$, we have uniform boundedness of all variables.

3. Numerical approach

With a view to solving the above non-dimensional equations, we use an embedded Runge-Kutta (RK) technique, namely the RKAHeM (4, 4) technique, for its ability to achieve efficient results. A detailed description of the RKAHeM (4, 4) technique is presented in the next subsection.

3.1. RKAHeM (4, 4) technique

A concise overview of the RKAHeM (4, 4) method is given below:

Consider the initial value problem (IVP) in the interval [a, b]

$$y(t) = \dot{f}(t, y(t)),$$

according to an initial assumption $y(a) = y_0$, in which the function $f: R \times R^m$ is close enough to the exact solution $(t, y(t)), t \in [a, b]$ to be sufficiently differentiable. To successfully resolve the system of equations given by $(4) - (6)$, an embedded RK (4, 4) technique can be of help [6, 7]. The enhanced Butcher tableau of parameters shown in Table 1.1 can be used to represent a general s-stage RK pair.

Table 1.1: The Butcher Tableau (BT)

c	A
	b^T
	$\hat{b}^T$
	E^T

In Table 1.1, b^T, $\hat{b}^T$, and $c \in R^s$, and $A \in R^s \times R^s$. The y values are attained by the two techniques of interest at $x = x_n + 1$ can be stated in the way detailed below:

$$y_{n+1} = y_n + h\sum_{i=1}^{s} b_i k_i \qquad (7)$$

$$\hat{y}_{n+1} = y_n + h\sum_{i=1}^{s} \hat{b}_i k_i \quad (8)$$

Where h designates the size of the step,

$$k_i = f\left(x_n + c_i h, y_n + h\sum_{j=1}^{s} a_{ij}k_i\right)$$

$$c_i = h\sum_{j=1}^{s} a_{ij,\ i=1,2,3\ldots}$$

In the above equations, c, b, and $\hat{b}$ are s dimensional vectors and $A(a_{ij})$ is a matrix of order $s \times s$. In an embedded technique, the local truncation error (LTE) can be estimated through $LTE = y_{n+1} - \hat{y}_{n+1}$. It is suitable to note at this juncture that the LTE controls h [8]. For the method of four stages, the Butcher coefficient array can be displayed in the table below (see Table 1.2**)**

Table 1.2: The BT of the method of four stages.

	0			
c_2	a_{21}			
c_3	a_{31}	a_{32}		
c_4	a_{41}	a_{42}	a_{43}	a_{44}
	b_1	b_2	b_3	b_4

The well–known RKAM (Runge-Kutta 4th order arithmetic mean) approach can be displayed in the form of a Butcher array [8]. The BT of this procedure is detailed in Table 1.3.

Table 1.3: The BT of the RKAM (4, 4) method.

0				
$\frac{1}{2}$	$\frac{1}{2}$			
$\frac{1}{2}$	0	$\frac{1}{2}$		
1	0	0	1	0
1	$\frac{1}{6}$	$\frac{1}{3}$	$\frac{1}{3}$	$\frac{1}{6}$

The equivalent comparable equations describing the RKAM (4, 4) approach are shown in Table 1.3.

$$y_{n+1} = y_n + \frac{h}{6}[k_1 + 2k_2 + 2k_3 + k_4] \quad (9)$$

where

$$k_1 = f(x_n, y_n)$$
$$k_2 = f\left(x_n + \tfrac{1}{2}h, y_n + \tfrac{1}{2}hk_1\right)$$
$$k_3 = f\left(x_n + \tfrac{1}{2}h, y_n + \tfrac{1}{2}hk_2\right)$$
$$k_4 = f(x_n + h, y_n + hk_3)$$

The RKAM (4, 4) method with Butcher array, can also be put in the modified form, which is shown in Table 1.4.

Table 1.4: The BT of the revised RKAM (4, 4) approach.

0			
$\frac{1}{2}$	$\frac{1}{2}$		
$\frac{1}{2}$	0	$\frac{1}{2}$	
1	0	0	1
	$\frac{1}{3}$	$\frac{1}{3}$	$\frac{1}{3}$

Again, the RKHeM (4, 4) (Runge-Kutta heronian mean) method as in [9] can be presented as under:

$$y_{n+1} = y_n + \frac{h}{9}\left[k_1 + 2k_2 + 2k_3 + k_4 + \sqrt{k_1k_2} + \sqrt{k_2k_3} + \sqrt{k_3k_4}\right] \quad (10)$$

$$y_{n+1} = y_n + \frac{h}{9}\left[k_1 + 2k_2 + 2k_3 + k_4 + \sqrt{|k_1k_2|} + \sqrt{|k_2k_3|} + \sqrt{|k_3k_4|}\right] \quad (11)$$

where

$$k_1 = f(x_n, y_n)$$
$$k_2 = f\left(x_n + \tfrac{1}{2}h, y_n + \tfrac{1}{2}hk_1\right)$$
$$k_3 = f\left(x_n + \tfrac{1}{2}h, y_n - \tfrac{1}{48}hk_1 + \tfrac{25}{48}hk_2\right)$$
$$k_4 = f\left(x_n + h, y_n - \tfrac{1}{24}hk_1 + \tfrac{47}{600}hk_2 + \tfrac{289}{300}hk_3\right)$$

The synthesis of RKAM (4, 4) with that of RKHeM (4, 4) (Eqs. (9) and (10)) is to refer as RKAHeM (4, 4), and can be formulated as

$$y_{n+1} = y_n + \frac{h}{6}[k_1 + 2k_2 + 2k_3 + k_4] \quad (12)$$

$$y^*_{n+1} = y_n + \frac{h}{9}\left[k^*_1 + 2k^*_2 + 2k^*_3 + k^*_4 + \sqrt{|k^*_1k^*_2|} + \sqrt{|k^*_2k^*_3|} + \sqrt{k^*_3k^*_4|}\right] \quad (13)$$

where

$$k_1 = f(x_n, y_n)$$
$$k_2 = f\left(x_n + \tfrac{1}{2}h, y_n + \tfrac{1}{2}hk_1\right)$$
$$k_3 = f\left(x_n + \tfrac{1}{2}h, y_n + \tfrac{1}{2}hk_2\right)$$
$$k_4 = f(x_n + h, y_n + hk_3)$$
$$k^*_1 = k_1$$
$$k^*_2 = k_2$$
$$k^*_3 = f\left(x_n + \tfrac{1}{2}h, y_n - \tfrac{1}{48}hk_1 + \tfrac{25}{48}hk_2\right)$$
$$k^*_4 = f\left(x_n + h, y_n - \tfrac{1}{24}hk_1 + \tfrac{47}{600}hk_2 + \tfrac{289}{300}hk_3\right)$$

The Butcher tableau notation for the integrated RKAHeM (4, 4) technique may be presented in the form shown in Table 1.5.

Table 1.5: The BT corresponding to the RKAHeM (4, 4) method.

0		
$\frac{1}{2}$	$\frac{1}{2}$	
$\frac{1}{2}$	0	$\frac{1}{2}$

1	0	0	1
	…	…	…
	….	….	….
$\frac{1}{2}$	$\frac{-1}{48}$	$\frac{25}{48}$	
1	$\frac{-1}{24}$	$\frac{47}{600}$	$\frac{289}{300}$
	$\frac{1}{3}$	$\frac{1}{3}$	$\frac{1}{3}$
	$\frac{1}{3}$	$\frac{1}{3}$	$\frac{1}{3}$
	E^T		

Hence, by Butcher array (Table 1.1), one can write out

$$b^T = y_{n+1}^{AM} = y_n + \frac{h}{6}[k_1 + 2k_2 + 2k_3 + k_4] \quad (14)$$

$$\hat{b}^T = y_{n+1}^{HeM} = y_n + \frac{h}{9}\left[k_1^* + 2k_2^* + 2k_3^* + k_4^* + \sqrt{|k_1^* k_2^*|} + \sqrt{|k_2^* k_3^*|} + \sqrt{k_3^* k_4^*|}\right] \quad (15)$$

and the estimation of the LTE as

$$E^T = |b^T - \hat{b}^T|$$

The RKAHeM(4,4) algorithm executes in four stages to produce the solution, that characterized by a common set of vectors k_1 and k_2 using b^T and $\hat{b}^T$ roughly, but k_1 and k_2 use b^T while k_3^* and k_4^* use $\hat{b}^T$.

3.2. Algorithm for solving the system of IVP by RKHeM (4, 4) technique

The procedure for computing an approximate solution to the system of IVP is given by the system of Eqs. $(4) - (6)$, are depicted herein:

INPUT: endpoints a, b ; initial conditions x_0, y_0, v_0; tolerance, TOL: h.
OUTPUT: t, x, y, v.
Step 1: set $t = a$.
Step 2: while do steps $3 - 7$.
Step 3: set

$$k_1 = f_1(t_n, x_n, y_n, v_n)$$
$$m_1 = f_2(t_n, x_n, y_n, v_n)$$
$$p_1 = f_3(t_n, x_n, y_n, v_n)$$
$$k_2 = f_1\left(t_n + \frac{h}{2}, x_n + \frac{hk_1}{2}, y_n + \frac{hm_1}{2}, v_n + \frac{hp_1}{2}\right)$$
$$m_2 = f_2\left(t_n + \frac{h}{2}, x_n + \frac{hk_1}{2}, y_n + \frac{hm_1}{2}, v_n + \frac{hp_1}{2}\right)$$
$$p_2 = f_3\left(t_n + \frac{h}{2}, x_n + \frac{hk_1}{2}, y_n + \frac{hm_1}{2}, v_n + \frac{hp_1}{2}\right)$$
$$k_3 = f_1\left(t_n + \frac{h}{2}, x_n + \frac{hk_2}{2}, y_n + \frac{hm_2}{2}, v_n + \frac{hp_2}{2}\right)$$
$$p_3 = f_2\left(t_n + \frac{h}{2}, x_n + \frac{hk_2}{2}, y_n + \frac{hm_2}{2}, v_n + \frac{hp_2}{2}\right)$$

$$m_3 = f_3\left(t_n + \frac{h}{2}, x_n + \frac{hk_2}{2}, y_n + \frac{hm_2}{2}, v_n + \frac{hp_2}{2}\right)$$
$$k_4 = f_1(t_n + h, x_n + hk_3, y_n + hp_3, v_n + hm_3)$$
$$p_4 = f_2(t_n + h, x_n + hk_3, y_n + hp_3, v_n + hm_3)$$
$$m_4 = f_3(t_n + h, x_n + hk_3, y_n + hp_3, v_n + hm_3)$$
$$sk_1 = k_1$$
$$sm_1 = m_1$$
$$sp_1 = p_1$$
$$sk_2 = k_2$$
$$sm_2 = m_2$$
$$sp_2 = p_2$$
$$sk_3 = f_1\left(t_n + \frac{h}{2}, x_n - \frac{1}{48}hk_1 + \frac{25}{48}hk_2, y_n - \frac{1}{48}hm_1 + \frac{25}{48}hm_2, v_n - \frac{1}{48}hp_1 + \frac{25}{48}hp_2\right)$$
$$sm_3 = f_2\left(t_n + \frac{h}{2}, x_n - \frac{1}{48}hk_1 + \frac{25}{48}hk_2, y_n - \frac{1}{48}hm_1 + \frac{25}{48}hm_2, v_n - \frac{1}{48}hp_1 + \frac{25}{48}hp_2\right)$$
$$sp_3 = f_3\left(t_n + \frac{h}{2}, x_n - \frac{1}{48}hk_1 + \frac{25}{48}hk_2, y_n - \frac{1}{48}hm_1 + \frac{25}{48}hm_2, v_n - \frac{1}{48}hp_1 + \frac{25}{48}hp_2\right)$$
$$sk_4 = 7f_1\left(t_n + h, x_n - \frac{1}{24}hk_1 + \frac{47}{600}hk_2 + \frac{289}{300}hk_3, y_n - \frac{1}{24}hm_1 + \frac{47}{600}hm_2 + \frac{289}{300}hm_3, v_n - \frac{1}{24}hp_1 + \frac{47}{600}hp_2 + \frac{289}{300}hp_3\right)$$
$$sm_4 = 7f_2\left(t_n + h, x_n - \frac{1}{24}hk_1 + \frac{47}{600}hk_2 + \frac{289}{300}hk_3, y_n - \frac{1}{24}hm_1 + \frac{47}{600}hm_2 + \frac{289}{300}hm_3, v_n - \frac{1}{24}hp_1 + \frac{47}{600}hp_2 + \frac{289}{300}hp_3\right)$$
$$sp_4 = 7f_2\left(t_n + h, x_n - \frac{1}{24}hk_1 + \frac{47}{600}hk_2 + \frac{289}{300}hk_3, y_n - \frac{1}{24}hm_1 + \frac{47}{600}hm_2 + \frac{289}{300}hm_3, v_n - \frac{1}{24}hp_1 + \frac{47}{600}hp_2 + \frac{289}{300}hp_3\right)$$

Step 4:

$$xx_{n+1} = x_n + \frac{h}{6}[k_1 + 2k_2 + 2k_3 + k_4]$$
$$yy_{n+1} = y_n + \frac{h}{6}[m_1 + 2m_2 + 2m_3 + m_4]$$
$$vv_{n+1} = v_n + \frac{h}{6}[p_1 + 2p_2 + 2p_3 + p_4]$$
$$sx_{n+1} = xx_n + \frac{h}{9}\left[sk_1 + 2sk_2 + 2sk_3 + sk_4 + \sqrt{|sk_1sk_2|} + \sqrt{|sk_2sk_3|} + \sqrt{|sk_3sk_4|}\right]$$
$$sy_{n+1} = yy_n + \frac{h}{9}\left[sm_1 + 2sm_2 + 2sm_3 + sm_4 + \sqrt{|sm_1sm_2|} + \sqrt{|sm_2sm_3|} + \sqrt{|sm_3sm_4|}\right]$$
$$sv_{n+1} = vv_n + \frac{h}{9}\left[sp_1 + 2sp_2 + 2sp_3 + sp_4 + \sqrt{|sp_1sp_2|} + \sqrt{|sp_2sp_3|} + \sqrt{|sp_3sp_4|}\right]$$
$$ERREST1 = abs(xx_{n+1} - sx_{n+1})\frac{287}{331776}$$
$$ERREST2 = abs(yy_{n+1} - sy_{n+1})\frac{287}{331776}$$
$$ERREST3 = abs(vv_{n+1} - sv_{n+1})\frac{287}{331776}$$
$$ERREST = Max(ERREST1, ERREST2, ERREST3)$$

$$\delta_1 = \left(\frac{TOL}{2 \times ERREST1}\right)^{\frac{1}{4}}$$
$$\delta_2 = \left(\frac{TOL}{2 \times ERREST2}\right)^{\frac{1}{4}}$$
$$\delta_3 = \left(\frac{TOL}{2 \times ERREST3}\right)^{\frac{1}{4}}$$
$$\delta = \min[\delta_1, \delta_2, \delta_3]$$

Step 5: If ERREST ≤ TOL, then do step 6, step 7.
Step 6:

$$t_{n+1} = t_n + h$$
$$x_{n+1} = xx_n$$
$$y_{n+1} = yy_n$$
$$v_{n+1} = vv_n$$

Step 7: set $h = \delta h$.
Step 8: If $t > b$ then, set $h = b - t$ go to step (3), (4).
Step 9: OUTPUT (t, x, y, v).
Step 10: The procedure is complete.

3.3. Assessment of error regulation in RKAHeM (4, 4) method:

The key error components in numerical approximations of differential equations can be classified as truncation and rounding errors. The LTE and global truncation error (GTE) are studied in the following subsections.

Local Truncation Error: The LTE at the point x_{n+1} is the difference between the computed value x_{n+1} and the value at the point y_{n+1} on the solution curve that goes through the point (x_n, y_n).

Global Truncation Error: The GTE at the point x_{n+1} is defined as $y_{n+1} - y(x_{n+1})$, where $y(x)$ denotes the solution of the given IVP.

3.4. Local truncation error (LTE) for RKAHeM (4, 4) method

From Eq. (13), we obtain an estimate of LTE for the RKAHeM (4, 4) method as $LTE = y_{n+1} - y^*_{n+1}$, which may be used to control the step size h. The LTE for RKAM (4, 4) method is

$$y^{AM}_{n+1} = y_n + LTE_{AM},$$

and RKHeM (4, 4) method is

$$y^{HEM}_{n+1} = y_n + LTE_{HEM}.$$

The LTEs involves in the y derivatives of RKAM (4, 4) method and RKAHeM (4, 4) method arises, respectively,

$$LTE_{AM} = \frac{h^5}{2880}\left[-24ff_y^4 + f^4 f_{yyyy} + 2f^3 f_y f_{yyy} - 6f^3 f_{yy}^2 + 36f^2 f_y^2 f_{yy}\right] \quad (16)$$

$$LTE_{HEM} = \frac{h^5}{1658880}\left[19759ff_y^4 - 19926f^2 f_y^2 f_{yy} - 36576f^3 f_{yy}^2 - 13292f^3 f_y f_{yyy} + 576f^4 f_{yyyy}\right] \quad (17)$$

The absolute difference between LTE_{AM} and LTE_{HEM} is given by

$$|LTE_{AM} - LTE_{HEM}| = \frac{h^5}{1658880}\left[5935ff_y^4 + 40662f^2 f_y^2 f_{yy} + 33120f^3 f_{yy}^2 + 14442f^3 f_y f_{yyy}\right] \quad (18)$$

As in Lotkin [10], assuming the estimation below for f and its partial derivatives hold for $x \in [a, b]$ and $y \in (-\infty, \infty)$, we have

$$|f(x, y)| < Q, \left|\frac{\partial^{i+j} f(x,y)}{\partial x^i \partial y^j}\right| < \frac{p^{i+j}}{Q^{j-1}}, i + j \leq p \quad (19)$$

where p and Q are positive constants and p is the order of the method. In this case, $p = 4$. Hence,

using Eq. (18), we obtain

$$\left.\begin{array}{c} |f_y| < p \\ |f_x f f_y| < 2pQ \\ |f^4 f_y^4| < \frac{Q^4 p^4}{Q^3} \\ |f^4 f_{yyyy}| < \frac{Q^4 p^4}{Q^3} \\ |f^3 f_y f_{yyy}| < Q^3 p \frac{p^3}{Q^2} \\ |f^3 f_{yy}^2| < Q^3 \left(\frac{p^2}{Q}\right)^2 \\ |f^2 f_y^2 f_{yy}| < Q^2 p^2 \left(\frac{p^2}{Q}\right) \end{array}\right\} < p^4 Q$$

From Eqs. (18) and (19), we obtain

$$LTE_{AM} - LTE_{HEM} \leq \left(\frac{281}{331776}\right) p^4 Q h^5 \tag{20}$$

$$|y_{n+1}^{AM} - y_{n+1}^{HeM}| \leq \left(\frac{281}{331776}\right) p^4 Q h^5 \tag{21}$$

If we set out the tolerance as $TOL = 0.00005$, then by writing out $|y_{n+1}^{AM} - y_{n+1}^{HeM}| < TOL$, the error control and step size selection can be attained by Eq. (21) to give rise the formula

$$\frac{281}{331776} p^4 Q h^5 < TOL, or\ h < \left[\frac{1180.7 \times \text{TOL}}{p^4 Q}\right]^{1/5} \tag{22}$$

3.5. Global truncation error (GTE) for RKAHeM (4, 4) method

The Taylor series expansion up to h^5 at $x = x_n$ is set out as

$$y(x_n + h) = y(x_n) + hf + \frac{h^2}{2} f f_y + \frac{h^3}{6}\left(f f_y^2 + f^2 f_{yy}\right) + \frac{h^4}{24}\left(f^3 f_{yyy} + \frac{1}{6} f^2 f_y f_{yyy}\right) + \frac{h^5}{120}\left(f f_y^4 + f^4 f_{yyyy} + 7 f^3 f_y f_{yyyy} + 11 f^2 f_y^2 f_{yy} + f^3 f_{yy}^2\right) \tag{23}$$

The LTE for RKHeM (4, 4) is the difference between Eqs. (10) and (23),

$$LTE_{HEM} = \frac{h^5}{1658880}\left[19759 f f_y^4 - 19926 f^2 f_y^2 f_{yy} - 36576 f^3 f_{yy}^2 - 13292 f^3 f_y f_{yyy} + 576 f^4 f_{yyyy}\right] \tag{24}$$

By using the same procedure adapted as in [11] to evaluate the GTEs for the RKAM (4, 4) method and RKHeM (4, 4) method, respectively, given by

$$\in_{n+1} \leq \in_n + hL \in_n + \frac{h^2}{2} L \in_n + \frac{h^3}{6} L \in_n + \frac{h^4}{24} L \in_n + \frac{h^5}{1658880} y^v \zeta,$$

where $0 < \zeta < 1$,

$$|\in_{n+1}| \leq \left[1 + hL + \frac{h^2 L}{2} + \frac{h^3 L}{6} + \frac{h^4 L}{24}\right] |\in_n| + \frac{h^5}{1658880} M \leq [1 + c_1]| \in_n |B_1$$

where $c_1 = L\left(\sum \frac{h^{p-1}}{p!}\right) h$, $A_1 = 1 + c_1$, $B_1 = \frac{h^5}{1658880} M$, and $|y^v(x)| \leq M$.

A simple induction proof gives $|\in_n| \leq A_1^n |\in_0| + \left(\sum_{k=0}^{k-1} A_1^k\right) B_1$ i.e., for $A_1 \neq 0$, and $\in_0 = 0$, the term $| \in_n |$ can be written as

$$|\in_n| \leq \left(\frac{A_1^n - 1}{A_1 - 1}\right) B_1 \tag{25}$$

If we use the inequality $1 + x \leq e^x$, we get

$$A_1^n = (1 + c_1)^n = \left(1 + hL\left(\sum_{p=1}^{4} \frac{h^{p-1}}{p!}\right)\right)^n \leq e^{c_1 l} = e^{Lnh\left(\sum_{p=1}^{4} \frac{h^{p-1}}{p!}\right)} = e^{DL(x_n - x_0)} \tag{26}$$

where

$$D = \sum_{p=1}^{4} \frac{h^{p-1}}{p!}$$

By substituting Eq. (26), into the inequality (25) for ϵ, we obtain $|\in_n| \leq \left(\frac{h^4}{1658880}\right) M\left(e^{DL(x_n - x_0)}\right) - 1$ and, therefore, the GTE for the RKHeM (4,4) method is of order h^4. The LTE is a measure of the error incurred in the numerical solution produced by the given method. RKAHeM (4,4) outperforms the embedded centroidal, harmonic, and contra-harmonic means in terms of LTE, which consequently minimizes the error in the embedded Heronian mean. Based on the foregoing analysis, it can be inferred that if the LTE of a numerical method is $O\ (h^{p+1}\ )$, then the GTE is $O\ (h^p\ )$. Due to the lower accuracy relative to the LTE, the GTE cannot be reliably employed for error estimation or error control in practice.

3.6. Error estimation and automatic step size selection

It is worth pointing out that in the RKAHeM (4, 4) method with error control program, we choose the ERREST as the disparity between the outcomes obtained with the RKAM (4, 4) method and the HeM (4, 4) method. From Eq. (21), the error estimate (ERREST) is presented as

$$\text{ERREST} = |Y_{AM} - Y_{HeM}| \times \frac{287}{331776}. \tag{27}$$

Considering the above fact into account, we have solved the above system of Eqs. (4) − (6) by the RKAHeM (4, 4) technique, we attained numerical solutions which are illustrated graphically through figures which are discussed in the next section. Equations (4.4) − (4.6) are also solved by the RK (4, 4) method for comparison.

3.7. Sensitivity Analysis:

The following parameters from Equations (1) − (3) were selected for sensitivity analysis based on their biological significance and uncertainty in experimental measurement:

Parameter	Symbol	Baseline Value	Range Tested	Biological Interpretation
Target cell production rate	λ	2019 cells/ml/day	$1000 - 4000$	Rate of new target cell generation
Infectivity rate	β	3.25×10^{-7} ml/viral RNA copies/day	$10^{-8} - 10^{-6}$	Efficiency of viral entry into cells
Virus production rate	b	505 viral RNA copies/cell/day	$100 - 1000$	Rate of virion production by infected cells
Infected cell death rate	δ	$1/21$ per day	$1/42 - 1/10$	Lifespan of infected cells
Virus clearance rate	γ	6.73 per day	$3 - 15$	Rate of viral particle removal

Table 1.6: Viral kinetics model parameters.

Sensitivity Metrices: Three quantitative metrics were employed to assess parameter sensitivity. These are

- Peak Value Sensitivity: $S_{peak} = \frac{\partial(\text{Peak Value})}{\partial \text{p}} \times \frac{p}{Peak\ Value}$
- Steady-State Sensitivity: $S_{ss} = \frac{\partial(\text{Steady State})}{\partial \text{p}} \times \frac{p}{\text{Steady State}}$
- Timing Sensitivity: $S_{time} = \frac{\partial(\text{Time to Peak})}{\partial \text{p}} \times \frac{p}{\text{Time to Peak}}$

Summary of Findings:
The sensitivity analysis reveals that the target cell-limited model exhibits differential sensitivity to its five key parameters: the virus production rate (b) and the infectivity rate (β) are the most influential parameters, while the uninfected cell production rate (λ) and death rates (ρ, δ, γ) show moderate to low sensitivity. Importantly, the RKAHeM (4,4) method maintains numerical stability across all parameter variations, with error control mechanisms successfully adapting to both stiff and non-stiff regimes. The basic reproduction number (R_0) emerges as a critical composite parameter that largely determines the qualitative behavior of the system.

4. Inputs
For solving the system of equations $(1) - (3)$, the parameter value used are available in [12]. The outcomes are portrayed through figures 2 and 3. The used values are appended below.
$\lambda = 2019$ Cells/ (ml*day),
$\beta = 3.25 \times 10^{-7}$ ml/ (viral RNA copies*day),
$b = 505$ Viral RNA copies/ (cell*day),
$\rho = \delta = 1/21$ Per day, and
$\gamma = 6.73$ Per day.

5. Results and discussion
Numerical simulations of the target cell–limited viral dynamics model were carried out using both the classical fourth-order Runge–Kutta method (RK (4,4)) and the embedded Runge–Kutta–Albrecht–Heun–Euler method (RKAHeM (4,4)). The corresponding numerical solutions are presented graphically for comparison. For the RK (4,4) method, the temporal evolution of the uninfected and infected cell populations is illustrated in Fig. 2, while the dynamics of the free virus population are shown in Fig. 3. In the case of the RKAHeM (4,4) technique, the target and infected cell dynamics are depicted in Fig. 4, and the corresponding viral load evolution is presented in Fig. 5**.**
All population variables are expressed as percentages of their respective initial values. Time is nondimensionalized, where one unit of dimensionless time ($\tau = 1$) corresponds to 21 days. The parameter values used in the simulations are provided in the text and correspond to a basic reproduction number $R_0 = 2.17$ and treatment efficacy $\varepsilon = 0.007$.
From Figs. 2 and 3, it is observed that the uninfected target cell population remains nearly constant during the initial phase of infection. As viral particles begin to infect target cells, the number of infected cells increases rapidly, leading to a decline in the uninfected cell population. Eventually, both populations approach a steady-state configuration. The initial viral load was taken as 0.00307 viral RNA copies/ml. During the early stage, the viral population exhibits minimal variation; however, as virus-producing infected cells accumulate, the viral load increases sharply before stabilizing. When the system is solved using the RK (4,4) method, the viral population reaches a steady state at a constant level, as shown in Fig. 3. In contrast, the RKAHeM (4,4) method exhibits a more gradual stabilization process, with viral load values evolving within a bounded range before settling into steady-state behavior **(**Fig. 5). This indicates that the embedded method captures the transient dynamics more effectively.
To further assess accuracy, the numerical solutions obtained using RKAHeM (4,4) were compared with the corresponding analytical (exact) solutions. A root mean square error (RMSE) analysis was conducted to quantify the discrepancy between the RKAHeM (4,4) and RK (4,4) solutions. The maximum RMSE was found to be of order 10^{-1}, indicating satisfactory agreement between the numerical approaches. Notably, the embedded RKAHeM (4,4) method provides an intrinsic error control mechanism, which is not available in the classical fixed-step RK (4,4) scheme.
The improved performance of the RKAHeM (4,4) technique can be attributed to its variable step-size strategy, which allows the algorithm to adaptively refine the solution through additional iterations until the desired accuracy is achieved. Although this approach may require increased

computational effort and memory usage, such requirements are not prohibitive with modern digital computing resources. Consequently, the use of embedded numerical schemes, such as RKAHeM (4,4), offers a reliable and efficient framework for solving nonlinear systems arising in viral dynamics modeling.

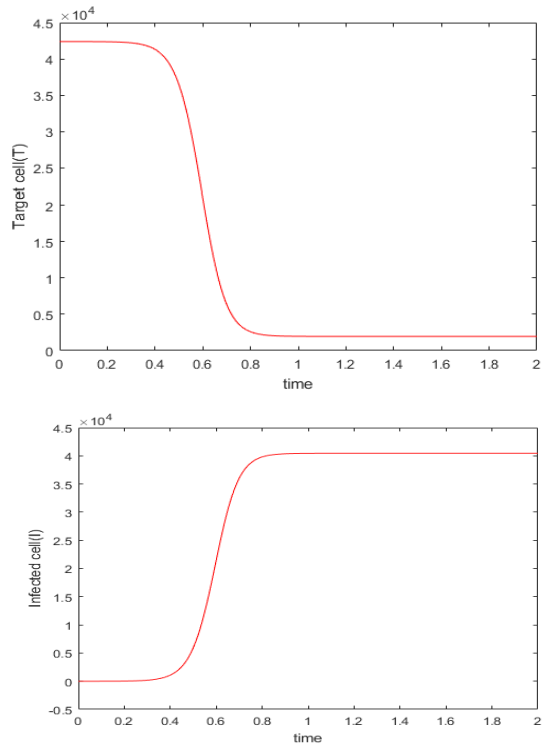

Figure 2**:** Temporal dynamics of uninfected target cells and infected cells obtained from the numerical solution of the viral dynamics model.

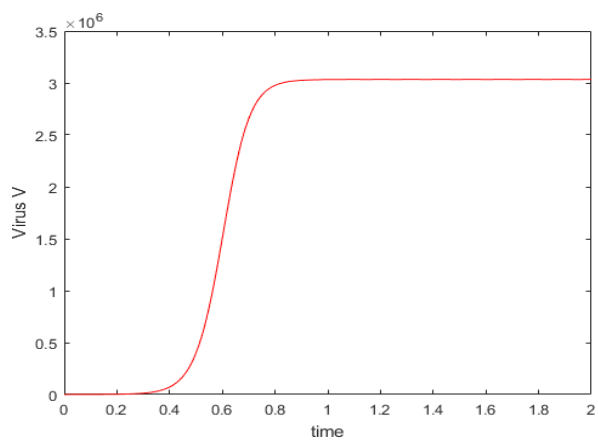

Figure 3: Simulated kinetics of free infectious particles derived from viral infection dynamics framework.

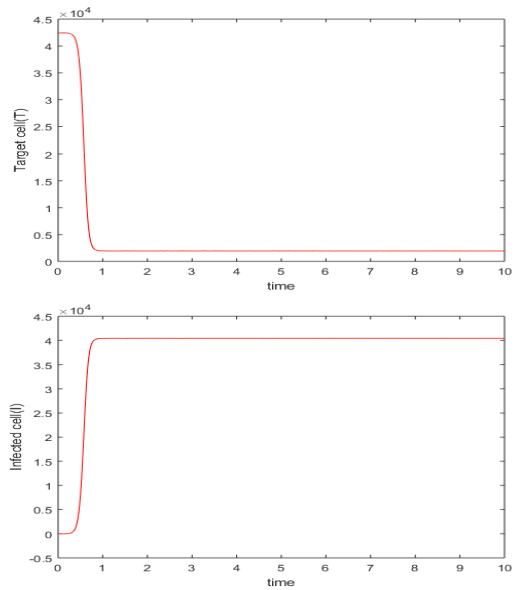

Figure 4: Comparative representation of target cell and infected cell populations.

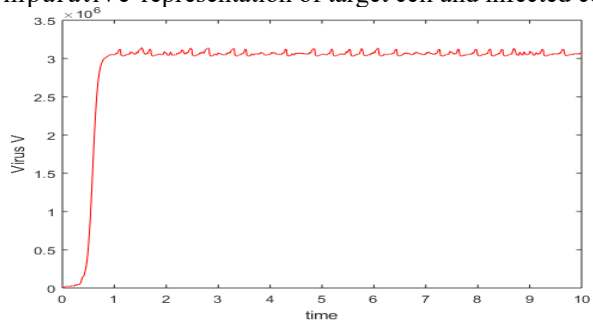

Figure 5: Progression of the systemic viral load simulated from the viral dynamics model.

6. Conclusion

This study demonstrates the crucial role of numerical solver selection in accurately simulating epidemiological models governed by nonlinear differential equations. Although both the classical fourth-order Runge–Kutta (RK (4,4)) method and the embedded RKAHeM (4,4) scheme produce reliable numerical solutions, the adaptive step-size control inherent in the RKAHeM (4,4) method yields improved accuracy and enhanced representation of biologically meaningful steady-state dynamics. The embedded approach effectively captures transient behavior and stabilizing viral dynamics that may be inadequately resolved by fixed-step methods. Consequently, for high-fidelity numerical simulations of complex viral dynamics and other nonlinear biological systems, adaptive embedded numerical solvers such as RKAHeM (4,4) are strongly recommended. The RKAHeM (4,4) method demonstrates superior accuracy per unit computational cost when compared to the classical RK4 and Implicit Euler. While the industry-standard adaptive solvers (RKF45 and ODE45) are robust and efficient, the RKAHeM (4,4) method shows slightly better performance in capturing the transient dynamics of the target cell-limited model, specifically during the peak infection phase. This is attributed to the RKAHeM (4,4) method's unique error estimation mechanism, which combines the Arithmetic Mean and Heronian Mean, providing a more sensitive

error control during rapid changes in the solution.

Declarations

Author contribution statement

Mst. Samira Khatun: Conducted the experimental work; Analyzed and interpreted the data; Wrote the paper.

Funding statement

This research did not receive any grant-in-aid from funding organizations in the public, private, or not-for-profit sectors.

Conflict of interest

The authors declare no conflict of interest.

References

[1] Kirui, J., Abidine, Y., Lenman, A., Islam, K., Gwon, Y. D., Lasswitz, L., et al. (2021). The phosphatidylserine receptor TIM-1 enhances authentic chikungunya virus cell entry. Cells, 10(7), 1828.

[2] DeBuysscher, B. L., Scott, D. P., Rosenke, R., Wahl, V., Feldmann, H., & Prescott, J. (2021). Nipah virus efficiently replicates in human smooth muscle cells without cytopathic effect. Cells, 10(6), 1319.

[3] Graw, F., & Perelson, A. S. (2016). Modeling viral spread. Annual Review of Virology, 3(1), 555.

[4] Iwasaki, A., & Medzhitov, R. (2020). Scared that COVID-19 immunity won't last? Don't be. The New York Times. https://www.nytimes.com/

[5] Anderson, R. M., & May, R. M. (1992). Infectious diseases of humans: Dynamics and control. Oxford University Press.

[6] Paul, G. C., & Senthilkumar, S. (2016). Execution of novel explicit RKARMS (4,4) technique in determining initial configurations of extra-solar protoplanets formed by disk instability. NRIAG Journal of Astronomy and Geophysics, 5(1), 1–8.

[7] Paul, G. C., Senthilkumar, S., & Pria, R. (2018). Storm surge simulation along the Meghna estuarine area: An alternative approach. Acta Oceanologica Sinica, 37(1), 40–49.

[8] Ponalagusamy, R., & Senthilkumar, S. (2009). A new method of embedded fourth order with four stages to study raster CNN simulation. International Journal of Automation and Computing, 6(3), 285–294.

[9] Wang, L. (2004). A new algorithm for solving classical Blasius equation. Applied Mathematics and Computation, 157(1), 1–9.

[10] Handel, A., Longini, I. M., Jr., & Antia, R. (2010). Towards a quantitative understanding of the within-host dynamics of influenza A infections. Journal of the Royal Society Interface, 7(42), 35–47.

[11] Yaakub, A. R., & Evans, D. J. (1999). A fourth-order Runge–Kutta RK(4,4) method with error control. International Journal of Computer Mathematics, 71(3), 383–411.

[12] Schwartz, E. J., Vaidya, N. K., Dorman, K. S., Carpenter, S., & Mealey, R. H. (2018). Dynamics of lentiviral infection in vivo in the absence of adaptive immune responses. Virology, 513, 108–113.